

The Micromechanics of Biological and Biomimetic Staggered Composites

Sacheen Bekah, Reza Rabiei, Francois Barthelat

Department of Mechanical Engineering, McGill University, 817 Sherbrooke Street West, Montreal, QC H3A 2K6, Canada

Abstract

Natural materials such as bone, tooth and nacre achieve attractive properties through the “staggered structure”, which consists of stiff, parallel inclusions of large aspect ratio bonded together by a more ductile and tougher matrix. This seemingly simple structure displays sophisticated micromechanics which lead to unique combinations of stiffness, strength and toughness. In this article we modeled the staggered structure using finite elements and small Representative Volume Elements (RVEs) in order to explore microstructure-property relationships. Larger aspect ratio of inclusions results in greater stiffness and strength, and also significant amounts of energy dissipation provided the inclusions do not fracture in a brittle fashion. Interestingly the ends of the inclusions (the junctions) behave as crack-like features, generating theoretically infinite stresses in the adjacent inclusions. A fracture mechanics criterion was therefore used to predict the failure of the inclusions, which led to new insights into how the interfaces act as a “soft wrap” for the inclusions, completely shielding them from excessive stresses. The effect of statistics on the mechanics of the staggered structure was also assessed using larger scale RVEs. Variations in the microstructure did not change the modulus of the material, but slightly decreased the strength and significantly decreased the failure strain. This is explained by strain localization, which can in turn be delayed by incorporating waviness to the inclusions. In addition, we show that the columnar and random arrangements, displaying different deformation mechanisms, lead to similar overall properties. The guidelines presented in this study can be used to optimize the design of staggered synthetic composites to achieve mechanical performances comparable to natural materials.

Keywords: biological materials, biomimetics, representative volume element, fracture mechanics, finite element analysis

Copyright © 2012, Jilin University. Published by Elsevier Limited and Science Press. All rights reserved.

doi: 10.1016/S1672-6529(11)60145-5

1 Introduction

Structural biological materials boast remarkable mechanical performances^[1,2], and they now serve as model for the development of novel bio-inspired engineering materials^[3–6]. Natural materials such as bone, teeth, seashells or spider silk are of interest because of their unique and attractive combinations of stiffness, strength and toughness. The building blocks of these materials are inherently weak, in the sense that they have a low strength and a large brittleness. The properties of these ingredients are, however, amplified by finely tuned microstructures, in order to achieve structural performance at the macroscale^[7]. Fig. 1 summarizes some key properties for bone and nacre, both made of organic materials “reinforced” by minerals. The modulus of these materials is lower than the stiff minerals, but their strength is similar or greater than that of the constituents. The most impressive improvement in bone and nacre is

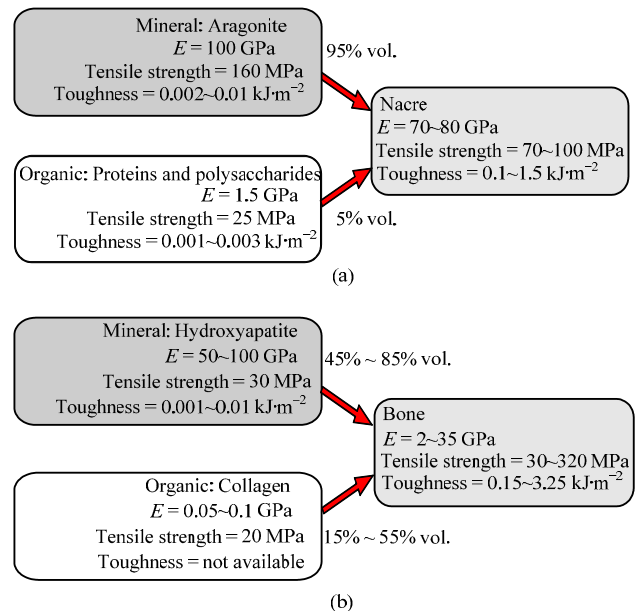


Fig. 1 Modulus, strength and toughness of (a) nacre and (b) bone, and of their “building blocks”. Data compiled from Refs. [2, 11–19].

Corresponding author: Francois Barthelat

E-mail: francois.barthelat@mcgill.ca

toughness, which is several orders of magnitude higher than that of each of the constituents. It is therefore critical to characterize the microstructures of these materials and their associated deformation and failure mechanisms. Interestingly, evolutionary processes have converged to a “universal pattern”^[8,9] in these materials, consisting of stiff inclusions of high aspect ratio (fibers or tablets) aligned along a single direction and overlapping over a fraction of their length (Fig. 2). This staggered structure has been shown to be optimum to achieve both stiffness and energy absorption^[10]. This seemingly simple structure displays sophisticated micromechanics which also leads to high toughness^[11].

The effect of the shape, size, aspect ratio and arrangement of these inclusions has been studied for nacre, the inner layer of some mollusks shells including bivalves, gastropods and cephalopods^[10,11,20–23] and/or for bone^[15,24–28], spider silk^[8] and diatom^[29]. The effect of the staggered structure is perhaps the most prominent in nacre, which is composed of 95% vol. of mineral inclusions forming a three-dimensional brick wall bonded by thin layers of proteins and polysaccharides^[30,31]. In nacre the mineral inclusions have the shape of polygonal microscopic tablets, which overlap each other by a well-defined distance in columnar nacre or randomly in sheet nacre (Fig. 2)^[12,13].

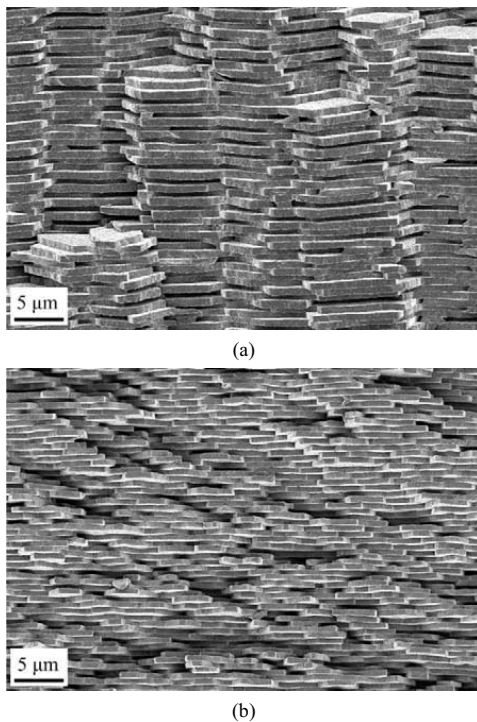


Fig. 2 Tablets arrangement for (a) columnar and (b) sheet naces^[12,13].

Under tensile loading along the direction of the tablets the stresses are channeled through tension in the tablets and shear at the softer interfaces^[13,15]. As the applied load increases, the interfaces yield in shear and tablets start to slide on one another over large volumes in the material. This key mechanism enables large deformations and energy dissipation^[32], making nacre 3000 times tougher than the mineral (in energy terms)^[2,33]. The sliding mechanism is very stable in these materials, because it is resisted by several mechanisms and features: the organic material which acts as tough adhesive^[32,34], mineral nanoasperities on the surface of the tablets which produce roughness^[35], and mineral bridges acting as reinforcements at the interface^[36]. The surfaces of the tablets also show significant waviness which impedes sliding where the adjacent tablets have to climb over one another, hence generating strain hardening, dissipating energy over larger volumes and delaying localization^[12]. An important requirement to achieve these properties is that the tablets must not fracture. Indeed, a successful staggered composite like nacre predominantly deforms by sliding of the tablets on one another, with limited occurrence of brittle fracture of the tablets^[13].

Interestingly, the staggered structure also exists in bone at the nanoscale, where hydroxyapatite platelets form a staggered array of reinforcing particles within individual collagen fibrils^[24]. The fibrils themselves form a staggered structure, and in-situ X-ray experiments have suggested that, similar to nacre, the sliding of the fibrils on one another is generating the large inelastic strains observed in bone at the macroscale^[24]. The staggered structure is also reminiscent of layered composites^[37], while some of the mechanisms associated with the high aspect ratio of each tablet are similar to those found in fiber composites^[38,39]. However, the unique mechanism of sliding and energy dissipation is only found in nature, and is virtually absent in engineering materials. The prospect of materials with enhanced stiffness, hardness and toughness has motivated the development of several “artificial naces” with promising fabrication techniques^[40–44]. Improvements in mechanical performance were achieved in these materials, mostly benefiting from crack deflection. However, the highly controlled collective tablet sliding and the associated energy dissipation could not be duplicated, except in large scale model materials made of millimeter size tablets^[4,42].

In order to fully harness the unique mechanisms associated with the staggered structure in engineering materials, design and optimization are essential^[40]. To this end, models that capture the effect of the staggered microstructure on modulus and strength are required. In addition, detrimental failure modes such as tablet fracture must be accurately predicted so they can be prevented at the design stage. Some of these questions have partially been answered for nacre and bone^[45–47]. These models typically involve two-dimensional Representative Volume Elements (RVEs)^[15,22] to capture the load transfer from shear at the interface to tension in the tablets. Proper scaling of the staggered structure is also critical. According to the Griffith criterion of fracture mechanics, decreased flaw size results in high tensile strength for a brittle component. Since any given component can only contain flaws that are smaller than its dimension, the Griffith criterion predicts that smaller objects are stronger. Following these principles Currey^[48] put forth the idea that the size of the defects in the minerals cannot be greater than the small size of the mineral inclusions, which therefore makes them stronger. More recently, the idea was further developed by Gao and co-workers^[20], who argued that nanoscale tablets approach the theoretical strength of the mineral.

The aim of this article is to provide a full picture of the effect of inclusion aspect ratio, shape and size on the sliding mechanism of the inclusions. This work completes studies on collective sliding mechanisms and toughening effects that have been published previously^[11,13,49], providing unified guidelines for the design of engineering materials based on the staggered configuration. First, the mechanical response of small two-dimensional RVEs of the staggered structure is studied through analytical solutions and finite elements. Detailed parametric studies on key structural parameters and their effects on the modulus and the strength reveal the “design maps” useful in the design of artificial biomimetic materials. The issue of tablet fracture as a detrimental failure mode is examined, where detailed stress analysis leads to a novel scaling law for these materials. Finally, the effect of inclusion morphology (waviness and nano-asperities) on the stress-strain curve is explored.

2 Staggered flat inclusions

A basic two-dimensional RVE can be used to obtain the basic properties of the staggered structures^[15,22]

(Fig. 3). In this section we review the main analytical models for modulus, strength and energy absorption, and we compare them with a finite element model. The model is two-dimensional based on plane strain assumption. Periodic boundary conditions^[12] are imposed on the edges of the model. The RVE contains linear elastic tablets (modulus E_t , Poisson's ratio ν , length L , thickness t) which are staggered and overlap the tablets of the next layer by a length L_0 . The tablets are bonded by thin interfaces of a softer and more ductile material (tensile modulus E_i , shear modulus G_i , shear strength τ_i , thickness t_i). The ends of the tablets also meet along vertical lines called junctions. The junctions are free surfaces in the first case we considered, whereas in the second case the interface material is also present at the junctions (“cohesive junctions” case). The model was then placed in uniaxial tension along the direction of the tablets. This RVE therefore captures the load transfer from tension in the tablets to shear at the interface, and the tensile load carried at the junctions for the models with cohesive junctions.

A large number of finite element models of the RVE with various combinations of structural parameters were automatically generated using MATLAB (Version R2009a, The MathWorks Inc.) and executed using ABAQUS (Version 6.8-3, ABAQUS, inc. Providence RI). Nacre served as model for the properties used in these models. Each tablet was modeled as linear elastic ($E_t = 100 \text{ GPa}$ ^[12] and $\nu = 0.2$, a typical value for ceramics and minerals), with linear plane strain elements. Plane strain was chosen to be consistent with a thick slab of material, theoretically infinite in the out-of-plane direction. While quantitative results may be slightly different if plane strain assumption is changed to plane stress, the qualitative effects of the microstructure on the overall performance will follow the same trends. To model the interfaces, cohesive elements were inserted between the

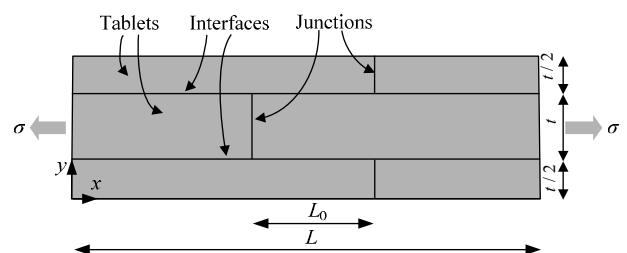


Fig. 3 Schematic of a RVE showing the microstructure dimensions (adapted from Refs. [21,22]).

tablets using the ABAQUS user element subroutine UEL. The associated cohesive law was previously used for natural nacre^[12]: A short linear elastic region was followed by a long plateau at a constant strength ($\tau_i = 25$ MPa) and a progressive decrease down to complete extinction of the cohesive force at 600 nm (Fig. 4a). Note that the behavior of the thin interface is assumed to be dominated by stretching of molecules^[32] which behave as independent springs across the interface^[12]. In order to avoid the interpenetration of the tablets, a compressive traction-separation law was superimposed^[12]. The models were periodic in both the longitudinal and transverse directions, while an average strain was imposed along the longitudinal direction to simulate uniaxial tension along the directions of the tablets. Fig. 4b shows a typical stress-strain response of the RVE, which, as expected, closely follows the shape of the cohesive law. The initial linear elastic region (elastic modulus E_c) is followed by a long plateau (strength σ_s). Sixty finite element models were constructed to explore various combinations of L/t (from 4 to 24) and L_0/L (from 0.05 to 0.5).

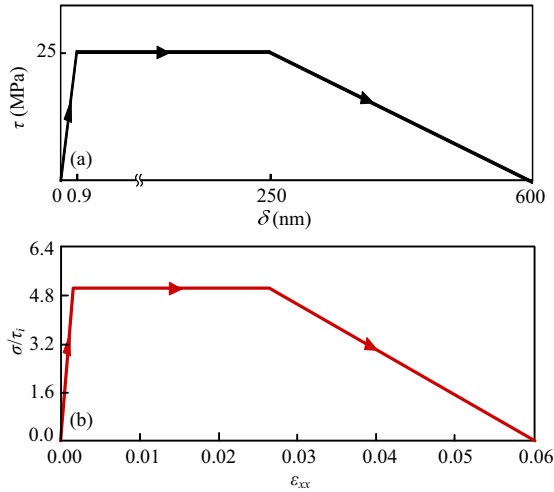


Fig. 4 (a) Cohesive law at the interface^[12], the horizontal axis was broken so that the end of the elastic region (0.9 nm) and the failure openings (250 nm and 600 nm) appear on the figure; (b) Stress strain response of an example RVE where $L/t = 20$, $L_0/L = 0.2$, $t_i/t = 0.06$, $E_i/G_i = 2$, $E_i/E_t = 0.015$ and $\nu = 0.2$.

2.1 Elastic modulus

Kotha *et al.*^[22] derived the elastic modulus for this RVE, but only for the case where $L_0 = L/2$ and with free junctions. Here we used a more general expression that includes cases where $0 \leq L_0 \leq L/2$ and that for cohesive ($k = 1$) or free ($k = 0$) junctions^[50]. The modulus E_c of the RVE is given by

$$E_c = \frac{t}{t + t_i} \frac{1}{\left(\frac{1}{E_i} + \frac{t_i}{L} \frac{1}{kE_i + G_i/N} \right)}, \quad (1)$$

where

$$N = \frac{1}{2} \alpha t \left[\frac{1 + \cosh(\alpha L_0)}{\sinh(\alpha L_0)} + \frac{1 + \cosh(\alpha(L - L_0))}{\sinh(\alpha(L - L_0))} \right],$$

and

$$\alpha = 2 \sqrt{\frac{G_i}{t t_i E_i}}.$$

The maps of modulus are displayed in Fig. 5 for a fixed value of $t_i/t = 0.06$ (i.e. fixed mineral concentration). The modulus increases with the aspect ratio L/t and overlap ratio L_0/L . Interestingly the modulus becomes almost independent of the overlap ratio when the overlap ratio becomes greater than 0.25. Comparing Fig. 5a and 5b, the addition of cohesive junctions clearly stiffens the composite by about 75% to 100%. The agreement between analytical and finite element results is reasonable, the two predictions being the closest for smaller tablet aspect ratios. The analytical prediction for the modulus therefore provides an adequate guideline to design a staggered composite for stiffness.

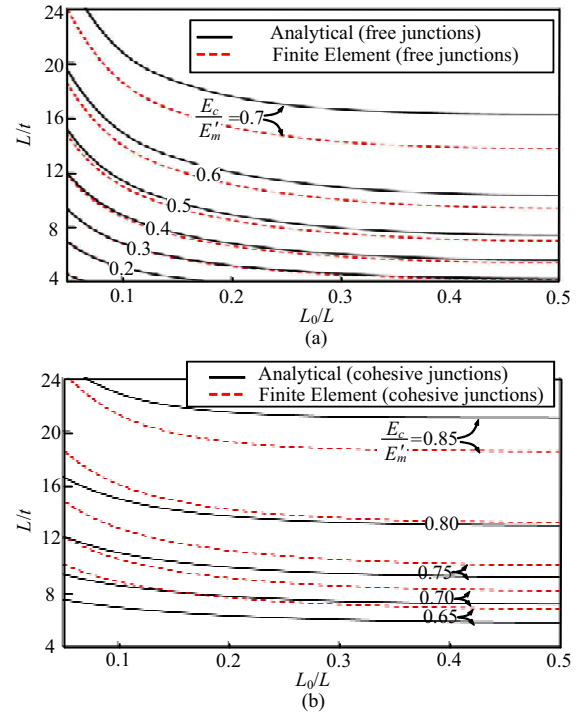


Fig. 5 Maps of elastic modulus from the analytical and finite element models for various combinations of L/t and L_0/L ($t_i/t = 0.06$, $E_i/G_i = 2$, $E_i/E_m = 0.015$ and $\nu = 0.2$), (a) free junctions, (b) cohesive junctions.

2.2 Strength

The tensile strength was assumed to be reached when the junctions and the overlap region of the interface have entirely failed, which is consistent with failure criteria used for ductile engineering materials. Assuming a constant strength in the post-yield region, the shear stress at the interfaces and the tensile stress at the junctions are uniform, and the strength of the composite σ_s is found by applying a simple force balance

$$\sigma_s = \tau_i \left[\frac{L_0}{t} + k \right], \quad (2)$$

where $k = 1$ is for the case of cohesive junctions and $k = 0$ is for the case of free junctions. The tensile strength and the shear strength of the ductile material are assumed to be the same, consistent with a model of the adhesive consisting of springs in parallel^[12].

Fig. 6 shows the predicted tensile strength of the composite with free and cohesive junctions. The predictions between analytical and finite element models are identical, which indicates that Eq. (2) is exact. Similar to modulus, the strength increases with the aspect ratio and/or the overlap ratio of the tablets. Cohesive junctions also strengthen the composite, as indicated by Eq. (2) and Fig. 6.

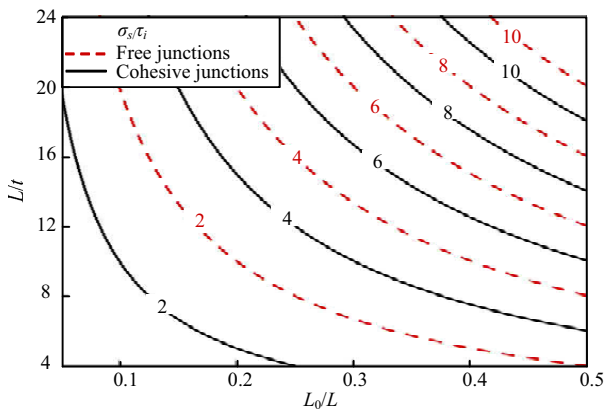


Fig. 6 Normalized tensile strength of the composite for various combinations of L/t and L_0/L ($t_i/t = 0.06$, $E_i/G_i = 2$, $E_i/E_m = 0.015$ and $\nu = 0.2$), (a) free junctions (dotted lines) and (b) cohesive junctions (solid lines).

2.3 Energy absorption

The advantage of the staggered structure is to combine stiffness, strength and energy absorption simultaneously. The energy absorbed per unit volume in the organic interface can be found from the area under the cohesive law divided by the thickness of the interface.

Since softening leads to strain localization, practically no energy can be dissipated by the interface in the softening region. For this reason we only consider the area under the cohesive law up to the interface separation at softening δ_s . Neglecting elastic deformations this calculation leads to

$$U_i \approx \frac{\tau_i \delta_s}{t_i}. \quad (3)$$

In turn, the energy per unit volume absorbed by the staggered structure can be written (neglecting elastic deformations and without considering the softening region):

$$U_c \approx \sigma_s \varepsilon_s, \quad (4)$$

where ε_s is the strain at softening. Using $\varepsilon_s \approx \delta_s/L$ and Eq. (2) leads to

$$\frac{U_c}{U_i} \approx \frac{t_i}{t} \left(\frac{L_0}{L} + \frac{t}{L} k \right). \quad (5)$$

Eq. (5) shows that the density of energy absorbed by the composite is smaller than that of the organic material. For example, for the typical values $L/t = 20$, $L_0/L = 0.2$, $t_i/t = 0.06$ and $k = 1$ (cohesive junctions), one finds $U_c/U_i \approx 0.015$. Eq. (5) shows that for a given energy absorption at the interface, larger energy absorption for the composite may be achieved by increasing the volume fraction of organic material (higher t_i/t) and increasing the overlap ratio L_0/L . For the case with cohesive junctions ($k = 1$), small aspect ratios L/t lead to higher energy absorption for the composite.

3 Tablet fracture

The models developed above show that increased overlap ratios L_0/L lead to higher strength, higher modulus and higher energy absorption. However, this also leads to higher tensile stress carried by the tablets, which may lead to their premature fracture. This failure mode is highly detrimental and should be avoided, because it is essential that the interfaces yield in order to make the most of their ductility and energy absorption capabilities.

For the failure analysis, regions of high tensile stresses were sought using finite elements. Fig. 7a shows that the tensile stresses in the tablets are the highest near the ends of the junctions, largely dominating any other region in the tablets. The accuracy of the analysis was

refined by refining the mesh in these areas, which led to ever increasing stresses with no apparent mesh convergence. This indicates that these points are actually stress singularities (infinite stresses), and that the junction (whether free or cohesive) act as crack-like features in the structure.

Fig. 7b shows the profile of the axial stress ahead of a crack-like junction. The stress is infinite at the tip of the junction ($x = 0$) and rapidly decreases for $x > 0$. The three plots clearly show the effect of the interfaces on the stress distribution within the tablets. In the case of rigid interfaces (i.e. the tablets are fused along their longer interfaces, but not at the junctions) the stresses for $x > 0$ are consistent with the asymptotic field for a mode I crack^[51]. When softer interfaces (i.e. lower τ_i) are introduced, the stresses still display a singularity at $x = 0$, but the magnitude for $x > 0$ greatly decreases. Overall the stresses are more uniformly distributed across the thickness, and as a result become higher than the rigid interface case for $x/t > 0.1$. Interestingly, Chan *et al.*^[37] studied a similar effect in multilayered ceramics bonded by ductile interfaces. Yielding of the interface, however, limits the amount of shear transferred and reduces the stress intensity factor in the tablets. In this context the ductile interfaces act as a “soft wrap” around each tablet, protecting them from excessive stresses since the highest possible stresses transmitted to the tablets are limited by the low strength of the interface. The stress singularity and the crack-like behavior of the junctions imply that a fracture mechanics criterion should be used to predict the brittle failure of the tablets. In this configuration the J -integral is path-dependant, because the tip of the junction intersects a softer interface, and the local stress field deviates slightly from a square root singularity. Nevertheless, fracture must be predicted in this case, and therefore the stress profiles ahead of the tip (Fig. 6b) were fitted with the asymptotic solution for a mode I crack^[51] in order to estimate K_I , the mode I stress intensity factor in the tablets. The resulting normalized stress intensity factor β as a function of L_0/t is shown in Fig. 8. The case of rigid interfaces (i.e. fused tablets) corresponds to the geometrical factor β for the case of a two-dimensional array of cracks. For small L_0/t the cracks are close enough to interact and the stress intensity factor is magnified. For $L_0/t > 2$ the system reduces to non-interacting one-dimensional arrays of collinear

cracks for which the theoretical geometrical factor is 1.13^[52]. Fig. 8 shows that when soft interfaces are introduced the decrease of stress intensity factor is significant for all values of L_0/t , which demonstrates how soft interfaces provide a soft, protective wrap around the tablets. The stress intensity is even further reduced by introducing cohesive junctions, which exert closure tractions on the crack-like junctions and shield the tablets from remotely applied stresses. For $L_0/t > 3$, however, the normalized stress intensity factor is almost identical with free and cohesive junctions.

The stress intensity factor from Fig. 8 can be predicted with the following simple equations

$$K_I = 0.58\tau_i\sqrt{t} \quad (\text{free junctions}), \quad (6)$$

$$K_I = 0.58\frac{L_0/t}{L_0/t+1}\tau_i\sqrt{t} \quad (\text{cohesive junctions}). \quad (7)$$

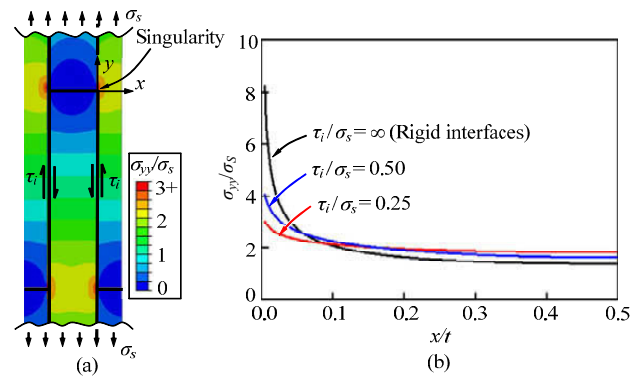


Fig. 7 (a) Contour plot of the axial stress in the RVE with flat tablets and free junctions, plotted at the beginning of the plateau region, when the applied stress is the highest ($L_0/t = 20$, $L_0/L = 0.2$, $t_i/t = 0.06$, $E_i/G_i = 2$, $E_i/E_t = 0.015$ and $\nu = 0.2$); (b) axial stress distribution ahead of the junction, normalized by the applied stress σ_s .

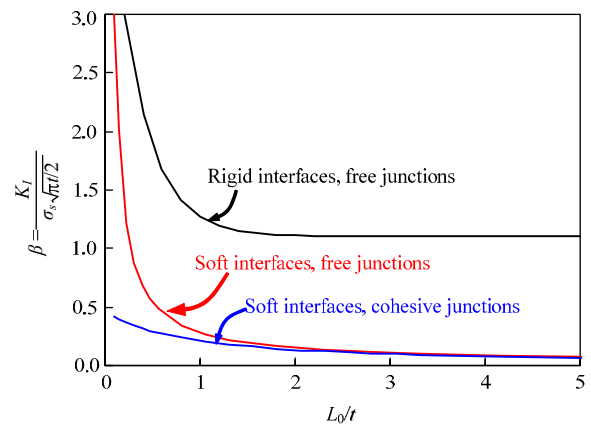


Fig. 8 Normalized stress-intensity factor in the tablets as function of L_0/t .

Note that mode I fracture is expected to be prominent for the tablets because of their brittleness, and therefore only this mode is considered to predict their failure. Eqs. (6) and (7) are extremely useful to determine the conditions that will prevent the fracture of the tablets (i.e. $K_I \leq K_{IC}$, the fracture toughness of the tablets). This condition leads to

$$0.58\sqrt{t} < \frac{K_{IC}}{\tau_i} \quad (\text{free junctions}), \quad (8)$$

$$0.58\sqrt{t} \left(\frac{L_0/t}{L_0/t+1} \right) < \frac{K_{IC}}{\tau_i} \quad (\text{cohesive junctions}). \quad (9)$$

Eqs. (8) and (9) were arranged so that the left hand sides contain information on microstructure while the right hand sides contain information on mechanical properties. From Eq. (8) it becomes evident that the fracture of the tablets can be prevented by using tough (high K_{IC}) and/or thin (small t) tablets, in combination with weak interfaces (low τ_i). Introducing cohesive junctions is also beneficial, but only if L_0/t is smaller than about 3.

4 Larger RVEs with statistics

While small RVEs are convenient to estimate basic mechanical properties, actual biological structures can display significant variations in microstructures, which naturally generates heterogeneities, weaker regions and stress concentrations. In this section the effect of statistics on the properties and micromechanics of the staggered structure is examined. Fig. 9 shows a large RVE of a staggered microstructure which was generated using Matlab (The MathWorks, Inc, USA). The model is composed of tablets with uniform thickness $t = 0.5 \mu\text{m}$ but with lengths following a normal distribution with mean $L = 10 \mu\text{m}$ and standard deviation $\Delta L = 1 \mu\text{m}$. The tablets were shifted from one layer to the next in order to generate a columnar arrangement with an overlap ratio of $L_0/L=0.25$ (Fig. 9). As a result of the statistical variations on tablet length, the overlap between the tablets also follows a statistical distribution. Cohesive elements with behavior similar to the previous section (Fig. 4a) were inserted at the interface and junctions. A uniaxial tension was then imposed on the RVE and simulated using ABAQUS on a supercomputing cluster (CLUMEQ, Montreal, Canada). Because of the stochastic nature of the model, different small RVEs ran-

domly generated could lead to different overall properties. For this reason, the size of the RVE was increased until several randomly generated models led to the same overall stress-strain curve. Sufficiently large RVEs could therefore properly capture the statistic of the microstructure.

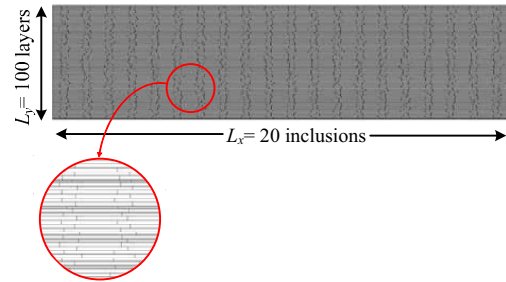


Fig. 9 Example of a large RVE with 20 inclusions by 100 layers where the inclusion lengths are normally distributed with mean and standard deviation $L^* = 10 \pm 1 \mu\text{m}$ and where the inclusions are stacked into columns with an overlap $L_0/L = 0.25$.

In addition to the columnar arrangement, another type of structure was obtained by modifying the algorithm used for model generation. The size of the inclusions was unchanged, but the overlap was achieved by randomly shifting the tablets from one layer to the next. This procedure led to a sheet arrangement, where the overlap L_0/L follows a uniform distribution: $0 \leq L_0/L \leq 0.5$. The average overlap ratio was therefore $L_0/L = 0.25$, the same as for the columnar case.

Fig. 10a shows the resulting stress-strain curve, which is similar in overall shape to the small RVE, where a linear elastic region is followed by inelastic deformation. The statistics, however, generates more “rounding” of the curve compared to those from the small RVE. The modulus for the columnar and sheet large RVE models is the same, and it is consistent with the value predicted by a small RVE model ($E = 89 \text{ GPa}$). The strength is slightly lower because failure occurs along the weakest cross-section in the model. In that sense, introducing statistics inevitably decreases the strength of the structure. The strain at failure ($\epsilon_f = 0.0035$) is also much smaller than the value predicted by a small RVE model ($\epsilon_S \approx 0.025$ for softening and $\epsilon_u \approx 0.06$ for ultimate failure). As soon as the strength of the model is reached, the inelastic deformations in the large RVE localize in a band perpendicular to the direction of loading (“columnar failure”, Fig. 10b). Failure strain and

energy absorption are therefore expected to be small for this configuration. The sheet model, which shows similar modulus, strength and strain at failure compared to the columnar model, follows a “stair” failure mode where the localization is more jagged because of the combination of high overlap and local shear stresses (Fig. 10c, as described and modeled in Ref. [13]).

Strain localization can be delayed by incorporating hardening in the cohesive law or by geometrical means through incorporating waviness to the tablets. Based on the two large RVEs described above a tablet waviness following a normal distribution was introduced using piecewise half-sinusoidal function with an amplitude of $75 \pm 15 \text{ nm}$ ($a = a_0 \pm \Delta a$) and a wavelength of $10.0 \pm 1.5 \text{ }\mu\text{m}$ ($\lambda = \lambda_0 \pm \Delta \lambda$).

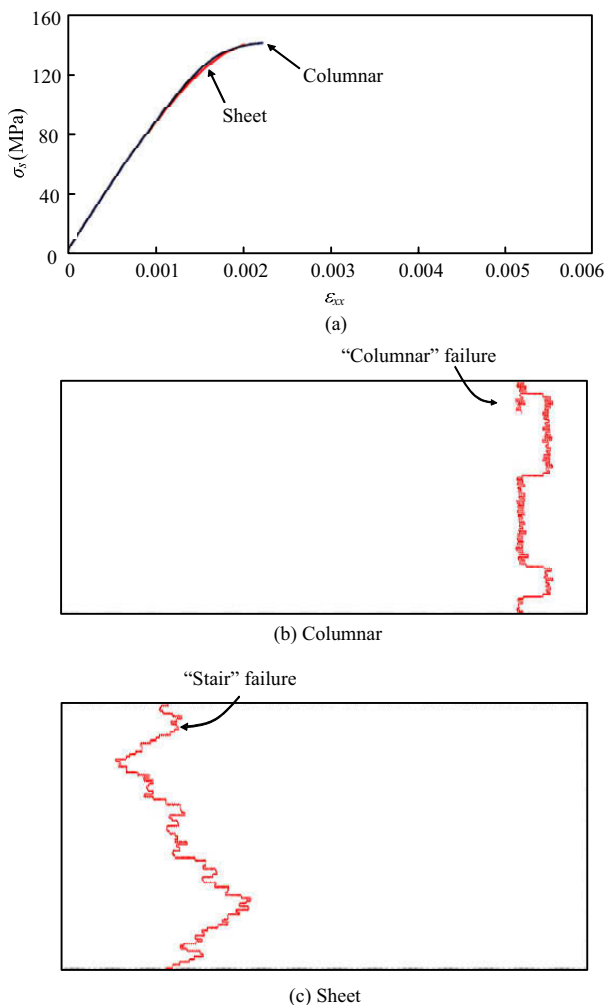


Fig. 10 (a) Comparison between the tensile response of the large RVEs with columnar and random (sheet) arrangements. Both configurations have an average overlap ratio of $L_0/L = 0.25$. (b and c) Plots of the failed cohesive elements at a strain $\epsilon_{xx} = 0.0025$; (b) columnar with $L_0/L = 0.25$; (c) random (sheet). Both configurations have an average overlap ratio of $L_0/L = 0.25$.

Fig. 11 shows the resulting stress-strain curves with snapshots of the corresponding microstructures. Interestingly the modulus and initial strength remained unchanged with the inclusion of the waviness. However, the post yield region showed that the strain hardening and localization observed for the flat tablet case was delayed. In the post yield region, the inelastic strains are more evenly distributed in the models (Fig. 12), which has implication for overall energy absorption, and also for the formation of large “process zones” of energy dissipation ahead of large cracks^[11].

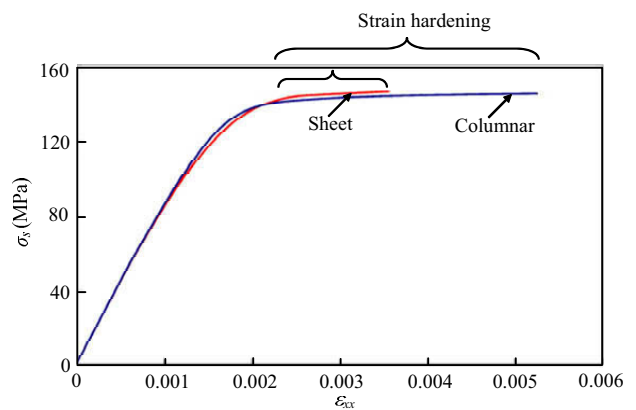


Fig. 11 Tensile response for columnar and sheet models with statistics in the length and waviness of the inclusions.

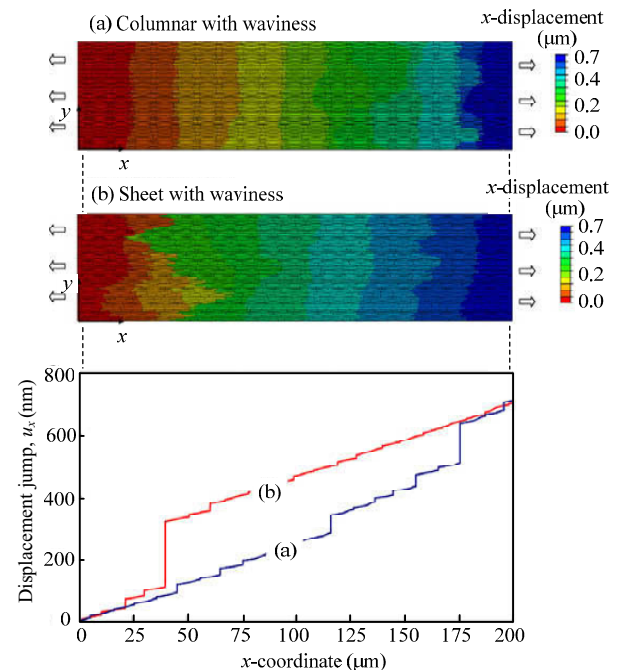


Fig. 12 Contours of the horizontal displacements u_x (along the loading direction) for (a) columnar and (b) sheet models. (c) Displacements u_x along the lower boundary of the models show different failure patterns (each step on this plot corresponds to a pair of inclusions separating). All data plotted at 0.35% macroscopic strain^[13].

5 Discussion and conclusion

Natural materials demonstrate how staggered composites can lead to attractive combinations of stiffness, strength and toughness. A high performance material like nacre is made of relatively poor ingredients and largely relies on the staggered arrangement of the structure to achieve attractive combinations of stiffness and toughness. The staggered structure is currently not used to its full potential in engineering materials, and the present study provides elements of designs for this powerful arrangement. Inclusions with high aspect ratio and with high overlap lead to the increase in the strength and modulus. These properties can be further enhanced by incorporating cohesive junctions at the ends of the inclusions. The overall tensile strength that can be achieved is, however, limited by the fracture of the inclusions. Eqs. (5) and (6) show the “soft-wrap” effect which protects the inclusions from excessive stresses. The interface must be sufficiently weak in order to achieve this effect. Slight statistical variations within the microstructure do not have a significant impact on modulus, but slightly lower strength and significantly decrease the strain at failure compared to the predictions from small RVEs. This demonstrates how the prediction of small RVEs can be deceived, because they are not capable of predicting localization. The potency of tablet waviness to delay localization is also highlighted in these models. Recent works have shown that nacre-like artificial structures can lead to interesting mechanical properties^[42]. The unified guidelines presented here can be utilized to optimize the design of similar staggered composites with high stiffness, strength and toughness, with great potential for actual engineering applications. The models can also be refined to incorporate mixed fracture modes at the interfaces and how they impact strength, energy dissipation and the fracture of the tablets themselves. Finally, structural hierarchy is well documented for other natural staggered composites, such as bone for example^[53], and recent studies show the profound impact of hierarchy on toughness^[10,29,54]. As such, the benefits of the staggered structure can be incorporated over several hierarchical length scales of the artificial designs, thereby achieving even further improvements in material properties.

Acknowledgments

This work was supported by the Faculty of Engineering at McGill University, the Natural Sciences and Engineering Research Council of Canada, the Canada Foundation for Innovation and the Fonds québécois de la recherche sur la nature et les technologies.

References

- [1] Meyers M A, Chen P Y, Lin A Y M, Seki Y. Biological materials: Structure and mechanical properties. *Progress in Materials Science*, 2008, **53**, 1–206.
- [2] Wegst U G K, Ashby M F. The mechanical efficiency of natural materials. *Philosophical Magazine*, 2004, **84**, 2167–2181.
- [3] Barthelat F. Biomimetics for next generation materials. *Philosophical Transactions of the Royal Society A*, 2007, **365**, 2907–2919.
- [4] Espinosa H D, Rim J E, Barthelat F, Buehler M J. Merger of structure and material in nacre and bone – Perspectives on de novo biomimetic materials. *Progress in Materials Science*, 2009, **54**, 1059–1100.
- [5] Vincent J F V, Bogatyreva O A, Bogatyrev N R, Bowyer A, Pahl A K. Biomimetics: Its practice and theory. *Journal of the Royal Society Interface*, 2006, **3**, 471–482.
- [6] Aizenberg J, Fratzl P. Biological and biomimetic materials. *Advanced Materials*, 2009, **21**, 387–388.
- [7] Ortiz C, Boyce M C. Materials science – Bioinspired structural materials. *Science*, 2008, **319**, 1053–1054.
- [8] Buehler M J, Keten S, Ackbarow T. Theoretical and computational hierarchical nanomechanics of protein materials: Deformation and fracture. *Progress in Materials Science*, 2008, **53**, 1101–1241.
- [9] Buehler M J, Yung Y C. Deformation and failure of protein materials in physiologically extreme conditions and disease. *Nature Materials*, 2009, **8**, 175–188.
- [10] Gao H J. Application of fracture mechanics concepts to hierarchical biomechanics of bone and bone-like materials. *International Journal of Fracture*, 2006, **138**, 101–137.
- [11] Barthelat F, Rabiei R. Toughness amplification in natural composites. *Journal of Mechanics and Physics of Solids*, 2011, **59**, 829–840.
- [12] Barthelat F, Tang H, Zavattieri P D, Li C M, Espinosa H D. On the mechanics of mother-of-pearl: A key feature in the material hierarchical structure. *Journal of the Mechanics and Physics of Solids*, 2007, **55**, 225–444.
- [13] Rabiei R, Bekah S, Barthelat F. Failure mode transition in

- nacre and bone-like materials. *Acta Biomaterialia*, 2010, **6**, 4081–4089.
- [14] Ji B H, Gao H J. Mechanical properties of nanostructure of biological materials. *Journal of the Mechanics and Physics of Solids*, 2004, **52**, 1963–1990.
- [15] Jäger I, Fratzl P. Mineralized collagen fibrils: A mechanical model with a staggered arrangement of mineral particles. *Biophysical Journal*, 2000, **79**, 1737–1746.
- [16] Wang R, Gupta H S. Deformation and fracture mechanisms of bone and nacre. *The Annual Review of Materials Research*, 2011, **41**, 41–73.
- [17] Currey J D. What determines the bending strength of compact bone? *Journal of Experimental Biology*, 1999, **202**, 2495–2503.
- [18] Ritchie R O, Kinney J H, Kruzic J J, Nalla R K. A fracture mechanics and mechanistic approach to the failure of cortical bone. *Fatigue & Fracture of Engineering Materials & Structures*, 2005, **28**, 345–371.
- [19] Broz M E, Cook R F, Whitney D L. Microhardness, toughness, and modulus of Mohs scale minerals. *American Mineralogist*, 2006, **91**, 135–142.
- [20] Gao H J, Ji B H, Jäger I L, Arzt E, Fratzl P. Materials become insensitive to flaws at nanoscale: Lessons from nature. *Proceedings of the National Academy of Sciences of the United States of America*, 2003, **100**, 5597–5600.
- [21] Jackson A P, Vincent J F V, Turner R M. The mechanical design of nacre. *Proceedings of the Royal Society of London*, 1988, **234**, 415–440.
- [22] Kotha S P, Li Y, Guzelsu N. Micromechanical model of nacre tested in tension. *Journal of Materials Science*, 2001, **36**, 2001–2007.
- [23] Rim J E, Zavattieri P, Juster A, Espinosa H D. Dimensional analysis and parametric studies for designing artificial nacre. *Journal of the Mechanical Behavior of Biomedical Materials*, 2011, **4**, 190–211.
- [24] Gupta H S, Seto J, Wagermaier W, Zaslansky P, Boesecke P, Fratzl P. Cooperative deformation of mineral and collagen in bone at the nanoscale. *Proceedings of the National Academy of Sciences of the United States of America*, 2006, **103**, 17741–17746.
- [25] Nikolov S, Raabe D. Hierarchical modeling of the elastic properties of bone at submicron scales: The role of extrafibrillar mineralization. *Biophysical Journal*, 2008, **94**, 4220–4232.
- [26] Dubey D K, Tomar V. Understanding the influence of structural hierarchy and its coupling with chemical environment on the strength of idealized tropocollagen–hydroxyapatite biomaterials. *Journal of the Mechanics and Physics of Solids*, 2009, **57**, 1702–1717.
- [27] Bar-On B, Wagner H D. Mechanical model for staggered bio-structure. *Journal of the Mechanics and Physics of Solids*, 2011, **59**, 1685–1701.
- [28] Liu G, Ji B, Hwang K-C, Khoo B C. Analytical solutions of the displacement and stress fields of the nanocomposite structure of biological materials. *Composites Science and Technology*, 2011, **71**, 1190–1195.
- [29] Sen D, Buehler M J. Structural hierarchies define toughness and defect-tolerance despite simple and mechanically inferior brittle building blocks. *Scientific Reports*, 2011, doi:10.1038/srep00035.
- [30] Currey J D, Taylor J D. The mechanical behavior of some molluscan hard tissues. *Journal of Zoology*, 1974, **173**, 395–406.
- [31] Schaeffer T E, Ionescu-Zanetti C, Proksch R, Fritz M, Walters D A, Almqvist N, Zaremba C M, Belcher A M, Smith B L, Stucky G D, Morse D E, Hansma P K. Does abalone nacre form by heteroepitaxial nucleation or by growth through mineral bridges? *Chemistry of Materials*, 1997, **9**, 1731–1740.
- [32] Smith B L, Schaeffer T E, Viani M, Thompson J B, Frederick N A, Kindt J, Belcher A, Stucky G D, Morse D E, Hansma P K. Molecular mechanistic origin of the toughness of natural adhesives, fibres and composites. *Nature*, 1999, **399**, 761–763.
- [33] Sarikaya M, Liu J, Aksay I A. Nacre: Properties, crystallography, morphology, and formation. In: Sarikaya M, Aksay I A (eds). *Biomimetics: Design and Processing of Materials*, AIP Press, Woodbury, NY, USA, 1995, 35–90
- [34] Meyers M A, Lin A Y M, Chen P Y, Mueyco J. Mechanical strength of abalone nacre: Role of the soft organic layer. *Journal of the Mechanical Behavior of Biomedical Materials*, 2008, **1**, 76–85.
- [35] Wang R Z, Suo Z, Evans A G, Yao N, Aksay I A. Deformation mechanisms in nacre. *Journal of Materials Research*, 2001, **16**, 2485–2493.
- [36] Song F, Bai Y L. Effects of nanostructures on the fracture strength of the interfaces in nacre. *Journal of Materials Research*, 2003, **18**, 1741–1744.
- [37] Chan K S, He M Y, Hutchinson J W. Cracking and stress redistribution in ceramic layered composites. *Materials Science and Engineering A*, 1993, **167**, 57–64.
- [38] Zok F W. Developments in oxide fiber composites. *Journal of the American Ceramic Society*, 2006, **89**, 3309–3324.
- [39] Evans A G. Perspective on the development of high-toughness ceramics. *Journal of the American Ceramic Society*, 1990, **73**, 187–206.

- [40] Bonderer L J, Studart A R, Gauckler L J. Bioinspired design and assembly of platelet reinforced polymer films. *Science*, 2008, **319**, 1069–1073.
- [41] Mayer G. New classes of tough composite materials – Lessons from natural rigid biological systems. *Materials Science & Engineering C*, 2006, **26**, 1261–1268.
- [42] Barthelat F. Nacre from mollusk shells: A model for high-performance structural materials. *Bioinspiration & Biomimetics*, 2010, **5**, 8.
- [43] Munch E, Launey M E, Alsem D H, Saiz E, Tomsia A P, Ritchie R O. Tough, bio-inspired hybrid materials. *Science*, 2008, **322**, 1516–1520.
- [44] Pai R K, Zhang L, Nykpanchuk D, Cotlet M, Korach C S. Biomimetic pathways for nanostructured poly(KAMPS)/ aragonite composites that mimic seashell nacre. *Advanced Engineering Materials*, 2011, **13**, B415–B422.
- [45] Budyn E, Hoc T, Jonvaux J. Fracture strength assessment and aging signs detection in human cortical bone using an X-FEM multiple scale approach. *Computational Mechanics*, 2008, **42**, 579–591.
- [46] Mercer C, He M Y, Wang R, Evans A G. Mechanisms governing the inelastic deformation of cortical bone and application to trabecular bone. *Acta Biomaterialia*, 2006, **2**, 59–68.
- [47] Nalla R K, Stolken J S, Kinney J H, Ritchie R O. Fracture in human cortical bone: Local fracture criteria and toughening mechanisms. *Journal of Biomechanics*, 2005, **38**, 1517–1525.
- [48] Currey J D. Mechanical properties of mother of pearl in tension. *Proceedings of the Royal Society of London*, 1977, **196**, 443–463.
- [49] Bekah S, Rabiei R, Barthelat F. Structure, scaling, and performance of natural micro- and nanocomposites. *BioNanoScience*, 2011, **1**, 53–61.
- [50] Yourdkhani M, Pasini D, Barthelat F. Multiscale mechanics and optimization of gastropod shells. *Journal of Bionic Engineering*, 2011, **8**, 357–368.
- [51] Lawn B R. *Fracture of Brittle Solids*, 2nd ed., Cambridge University Press, New York, USA, 1993.
- [52] Tada H, Press ASME, Irwin G R. *The Stress Analysis of Cracks Handbook*, 3rd ed., ASME press, New York, NY, USA, 2000.
- [53] Rho J Y, Kuhn-Spearing L, Zioupos P. Mechanical properties and the hierarchical structure of bone. *Medical Engineering & Physics*, 1998, **20**, 92–102.
- [54] Qin Z, Cranford S, Ackbarow T, Buehler M J. Robustness-strength performance of hierarchical alpha-helical protein filaments. *International Journal of Applied Mechanics*, 2009, **1**, 85–112.